

## Gamma-Rays and Neutrinos from Very Young Supernova Remnants

R.J. Protheroe, W. Bednarek\*, and Q. Luo  
Department of Physics and Mathematical Physics  
The University of Adelaide, Adelaide, Australia 5005  
\*permanent address: University of Łódź, 90-236 Łódź,  
ul. Pomorska 149/153, Poland.

### Abstract

We consider the result of acceleration of heavy ions in the slot gap potential of a very young pulsar with a hot polar cap. Photodisintegration of the heavy ions in the radiation field of the polar cap and pulsar surface gives rise to a flux of energetic neutrons. Some fraction of these neutrons interact with target nuclei in the supernova shell to produce neutrino and gamma-ray signals which should be observable from very young supernova remnants in our galaxy for a range of pulsar parameters.

## 1 Introduction

Young supernova remnants are probably sites of acceleration of particles to high energies and, as a result of interactions, also sources of high energy neutrinos and  $\gamma$ -rays [1–6]. Following the occurrence of SN1987A it was expected that high energy  $\gamma$ -rays would be detected from this object, but the observations have so far been negative [7–14]. Also, some models required the formation of a pulsar during the supernova (SN) explosion which has not yet been discovered. Nevertheless, SN1987A renewed interest in predicting neutrino and  $\gamma$ -ray fluxes from supernova remnants (SNR) for times soon after the explosion. For example, the model in which protons are accelerated of at the reverse shock which forms in a relativistic wind from a pulsar as a result of its confinement by the supernova envelope, proposed by Rees & Gunn [15], has been considered in several papers [4, 5, 16, 17]. In this model, relativistic protons produce  $\gamma$ -rays and neutrinos in collisions with the matter in the shell, and observable  $\gamma$ -ray fluxes were predicted for SN 1987A if the power in relativistic protons was  $\sim 10^{39}$  erg s $^{-1}$ . If the pre-supernova star had a strong wind, neutrinos and  $\gamma$ -rays could be produced in collisions of relativistic

particles accelerated by the supernova shock itself, with the surrounding matter. For this scenario, Kirk et al. [18] predicted detectable fluxes of TeV  $\gamma$ -rays for SN 1993J, but not for SN 1987A.

In the present paper, we consider yet another scenario in which particle acceleration along open magnetic field lines may take place in the pulsar magnetosphere if a neutron star with a high magnetic field and a sufficiently short period forms during the supernova explosion. That acceleration of heavy ions by the Crab pulsar may take place, has already been suggested, based on modeling the observed synchrotron wisps in the Crab nebula [19, 20]. In these papers it is proposed that a significant fraction of the rotational kinetic energy loss of the Crab pulsar is carried by ions which are injected with a rate close to the Goldreich & Julian current, and that these ions are accelerated through at least 20% of the total voltage available on open field lines.

It is expected that soon after supernova explosions the surface temperatures of newly formed neutron stars are much higher than derived from recent observations of the thermal emission from the surfaces of classical pulsars [21–23]. Just after formation, a neutron star’s surface temperature is expected to be very high ( $\sim 10^{11}$  K) but drop very rapidly, and models of neutron star cooling predict temperatures of the order of a few  $10^6$ – $10^7$  K during the first  $\sim 10$  years after the explosion [24, 25]. However, the polar cap of a neutron star can have a temperature  $\sim 10^7$  K or higher, due to the heating by electrons and  $\gamma$ -rays from cascades in the pulsar magnetosphere [26–28], and their thermal emission depends only on the pulsar parameters.

Nuclei, probably mainly Fe nuclei, extracted from the neutron star surface and accelerated to high Lorentz factors can be photodisintegrated during propagation through the neutron star’s radiation field. Relativistic neutrons extracted from Fe nuclei in this way propagate straight out and escape from the magnetosphere, interacting in or passing through the surrounding supernova remnant shell. Those interacting in the shell produce neutrino and  $\gamma$ -ray signals. Those passing through the shell decay into relativistic protons which contribute to the pool of Galactic cosmic rays.

In Sect. 2 we investigate the photodisintegration of nuclei in the radiation field of a pulsar. In Sect. 3 we consider the energetics of pulsars and the acceleration of particles in the slot gap, as well as polar cap heating. We then compute in Sect. 4 the spectrum of neutrons escaping from the pulsar’s radiation field, and in Sect. 5 the expected light curves and spectra of  $\gamma$ -rays and neutrinos. The acceleration of Fe nuclei in the outer gap of classical radio pulsars [29, 30], and photodisintegration of Fe on the nonthermal radiation of the outer gap is considered in another paper [31].

## 2 Photodisintegration of nuclei in pulsar thermal radiation

The possibility of photodisintegration of Fe nuclei during their propagation through thermal radiation from very young neutron stars has been noted by Bednarek & Karakuła [32].

The importance of this process can be evaluated by calculating the mean free path,  $\lambda_A(\gamma_A, T)$ , for relativistic nuclei with mass number  $A$  and Lorentz factor  $\gamma_A$  for photodisintegration, typically extracting one nucleon, in black body radiation with temperature  $T$  which is given by

$$\frac{1}{\lambda_A(\gamma_A, T)} = \int \int \frac{\epsilon^* n(\epsilon, T) \sigma_A(\epsilon^*)}{2\gamma_A \epsilon} d\epsilon d(\cos \theta), \quad (1)$$

where  $n(\epsilon, T)$  is the photon number density per unit photon energy at photon energy  $\epsilon$  for black body radiation at temperature  $T$ ,  $\sigma_A(\epsilon^*)$  is the cross section for photodissociation of a single nucleon from a nucleus with mass number  $A$  [33],  $\epsilon^* = \gamma_A \epsilon (1 - \beta_A \cos \theta)$  is the photon energy in the rest frame of the nucleus,  $\beta_A c$  is the velocity of the nucleus, and  $\theta$  is the angle between the direction of the nucleus and a thermal photon. In Fig. 1 we show, for illustration, the mean free paths through isotropic black body radiation with temperature  $T$ , for nuclei with various mass numbers as a function of Lorentz factor. Note that the mean free paths computed by us using Eq. 1 differ slightly for low  $A$  nuclei in comparison with those given by Karakuła & Tkaczyk [33] because the cross section given by Eq. 2 of their paper incorrectly separates the contributions from the Breit-Wigner peak and the approximately constant cross section at high energies.

The radiation field we adopt in the present work is anisotropic and the intensity of radiation at a particular point in space has the the following properties: in directions towards the neutrons star's polar caps the intensity is equal to that of black body radiation of temperature equal to that of the polar caps; in directions towards other parts of the the neutrons star's surface the intensity is equal to that of black body radiation of temperature equal to that of the surface; and in all other directions the intensity is zero. The radiation field may differ from this because of radiative transfer effects in the neutron star's atmosphere due to the presence of a strong magnetic field, and this may cause the intensity to depend on the angle to the magnetic pole (see e.g. ref. [34]). This effect may modify pulse profiles of pulsed X-ray emission, but it would not affect significantly the photodisintegration since the modulation with angle varies by a factor less than 4 for photon energies  $\sim 1$  keV (typical thermal photon energies for  $T = 10^7$  K).

To check if photodisintegration of Fe nuclei propagating in the anisotropic radiation field of a neutron star perpendicular to its surface is important, we compute the average number of neutrons extracted from Fe nuclei as a function of their Lorentz factor  $\gamma_{\text{Fe}}$ . We have made the reasonable approximation, that in every photodisintegration, only one nucleon is extracted. In Fig. 2(a) we show the average number of neutrons extracted from Fe nuclei as a function of Lorentz factor  $\gamma_{\text{Fe}}$  for different surface temperatures. It is clear that for a neutron star with a uniform surface temperature, the temperature needs to be rather high, above  $\sim 10^7$  K, for the process to occur efficiently. Such surface temperatures are higher than expected except within a few days of the explosion. However, as we shall discuss in a later section, neutron star polar caps may have very high temperatures due to particle acceleration and cascading in the magnetosphere. We show in Fig. 2(b) the average number of neutrons extracted from Fe nuclei as a function of Lorentz factor in

the radiation field of a heated polar cap of radius  $10^5$  cm for three temperatures, and we see that efficient photodisintegration can take place in such a radiation field.

We should point out that the presence of a magnetic field can have an effect on any process, including photodisintegration of nuclei by thermal photons, due to a change in kinematics, resonant effects, strong field particle wavefunctions, etc. In this paper, we neglect such effects which are probably small since heavy nuclei are involved. We shall, however, consider in the next section the possibility of photodisintegration of nuclei directly on the pulsar's magnetic field.

### 3 Photodisintegration of nuclei in the pulsar's magnetic field

The photodisintegration of iron nuclei may also occur because of the presence of an extremely high magnetic field. The component of magnetic field perpendicular to the direction of motion of a particle with velocity  $\beta c$  and Lorentz factor  $\gamma$ ,  $B_{\perp}(x, \gamma)$ , at distance  $x = \beta ct$  above the polar cap will give rise to electric and magnetic fields at time  $t' = t/\gamma$  in the particle's rest frame which are, in SI units,  $E'_{\perp}(t') = \gamma c B_{\perp}(x, \gamma)$  and  $B'_{\perp}(t') = \gamma B_{\perp}(x, \gamma)$  respectively. These fields are characteristic of electromagnetic radiation, and the time-integrated Poynting flux per unit angular frequency is

$$\frac{dF'}{dad\omega'} = \frac{2}{\mu_0 c} |E'_{\perp}(\omega')|^2, \quad (2)$$

where  $E'_{\perp}(\omega')$  is the Fourier transform of  $E'_{\perp}(t')$ , and the number of photons per unit area per unit angular frequency is

$$\frac{dN'}{dad\omega'} = \frac{1}{\hbar\omega'} \frac{2}{\mu_0 c} |E'_{\perp}(\omega')|^2. \quad (3)$$

This method is referred to as the Weizaeker-Williams method of virtual quanta (see Section 15.4 in ref. [35]).

As a relativistic iron nucleus travels along a magnetic field line with radius of curvature  $\rho$  it will acquire a drift velocity  $v_d$  perpendicular to the field direction with order of magnitude

$$v_d \sim \frac{c^2 \gamma}{\omega_B \rho}, \quad (4)$$

where  $\omega_B = 9.6 \times 10^7 ZB/A$  rad s<sup>-1</sup> is the non-relativistic cyclotron frequency and  $B$  is in Tesla (see e.g. ref. [35], p 587). Thus, the perpendicular component of magnetic field is given approximately by

$$B_{\perp}(x, \gamma) \approx \frac{v_d}{c} B(x). \quad (5)$$

We shall assume a dipole magnetic field

$$B(x) = B_s(R/r)^3 \quad (6)$$

where  $r \approx R + x$ ,  $R$  is the neutron star's radius, and we take the radius of curvature to be that of the last open field line [26]

$$\rho = 2 \left( \frac{rc}{\Omega} \right)^{1/2} \approx 1.4 \times 10^9 (r_8 P)^{1/2} \quad \text{cm} \quad (7)$$

where  $r_8 = r/10^8$  cm, and  $P$  is the period in s.

As a nucleus is extracted from the neutron star's surface and is accelerated along an open field line,  $B_\perp$  will initially increase as  $\gamma$  increases and then decrease as  $\rho$  increases and  $B$  decreases. In the instantaneous rest frame of the nucleus,  $B'_\perp$  (and  $E'_\perp$ ) will also increase from zero to some maximum, and then decrease. In the high  $\omega'$  limit, the the spectrum of virtual quanta will be determined by the most rapid change in  $E'_\perp = cB'_\perp$ . To see whether the presence of the pulsar's magnetic field is at all important for photodisintegration, we consider an extreme case:  $B_\perp$  changes instantaneously from zero to some constant high value,

$$B'_\perp(x, \gamma) \approx \Theta(0) \gamma_{\max} B_\perp(x=0, \gamma = \gamma_{\max}). \quad (8)$$

If enhanced photodisintegration due to the magnetic field is unimportant for this case, then we can safely neglect it in the present work.

For the case under consideration, the electric field in the instantaneous rest frame varies as

$$E'_\perp(t') \approx \Theta(0) E'_0 \quad (9)$$

where

$$E'_0 = \gamma_{\max} c B_\perp(x=0, \gamma = \gamma_{\max}). \quad (10)$$

Then

$$E'_\perp(\omega') \approx i \frac{E'_0}{2\pi\omega'} \quad (11)$$

where  $i = \sqrt{-1}$  and

$$\begin{aligned} \frac{dN'}{dad\omega'} &= \frac{1}{\hbar\omega'} \frac{2}{\mu_0 c} \left( \frac{E'_0}{2\pi\omega'} \right)^2 \\ &= \frac{1}{\pi\mu_0 c \hbar} E'^2_0 \omega'^{-3}. \end{aligned} \quad (12)$$

For a photodisintegration threshold of  $\hbar\omega'_{\min} \sim 30$  MeV ( $\omega'_{\min} \approx 4.6 \times 10^{22}$  rad s<sup>-1</sup>) we obtain an optical depth for photodisintegration on the magnetic field of

$$\begin{aligned} \tau_B &\approx \sigma_{\text{photo}} \int_{\omega'_{\min}}^{\infty} \frac{dN'}{dad\omega'} d\omega' \\ &\approx \sigma_{\text{photo}} \frac{1}{3\pi\mu_0 ch} E_0'^2 \omega'_{\min}{}^{-2}, \end{aligned} \quad (13)$$

where  $\sigma_{\text{photo}} \sim 10^{-26}$  cm<sup>2</sup> is an approximation to the energy-dependent photodisintegration cross section of Fe nuclei above threshold. Taking  $B_s = 1.414 \times 10^{12}$  gauss,  $P = 5$  ms,  $R = 1.2 \times 10^6$  cm, and  $\gamma_{\max} = 5 \times 10^7$ , we obtain  $E_0' \approx 5 \times 10^{19}$  V m<sup>-1</sup> giving  $\tau_B \approx 5 \times 10^{-7}$ . Clearly, photodisintegration of Fe nuclei on the pulsar's magnetic field is negligible for the presently assumed pulsar parameters.

## 4 Pulsar energetics and particle acceleration

We are interested in the case of a very young pulsar which has just been formed during a supernova explosion, and for a few years after formation. It is assumed that pulsar acceleration can operate very soon after the formation of a neutron star and can tap into a substantial fraction of the spin-down power that is not associated with gravitational radiation. We approximate this non-gravitational component of the spin-down power by the magnetic dipole radiation power (erg s<sup>-1</sup>) given by

$$L_{\text{em}}(\Omega, B) = B^2 R^6 \Omega^4 \sin^2 i / 6c^3, \quad (14)$$

where  $B$  is the surface magnetic field at the magnetic pole in G,  $R$  is the radius of the neutron star in cm,  $\Omega = 2\pi/P$  where  $P$  is the period in s, and  $i$  is the angle between the spin axis and rotation axis.

The total magnetic dipole spin-down power should also include the energy loss due to plasma flow (e.g. ref. [36]). However, pulsar spin-down through plasma winds is not well understood for the case of  $i \neq 0$ . Here, we use spin-down through dipole radiation as a working hypothesis and  $B \sin i$  is treated as one parameter (rather than having  $B$  and  $\sin i$  separately).

For the typical magnetic field of a classical pulsar  $B \sim 10^{12}$  G, for acceleration of ions up to sufficiently high energies for photodisintegration to take place we need to have a short initial period. Thus, in all the calculations we make in the present paper we shall adopt  $B \sin i = 10^{12}$  G, and an initial period of either  $P_0 = 5$  ms or  $P_0 = 10$  ms.

Equating  $L_{\text{em}}$  with the loss of rotational kinetic energy, the period at time  $t$  is given by the well-known formula,

$$P^2(t) = 1.04 \times 10^{-15} t B_{12}^2 \sin^2 i + P_0^2, \quad (15)$$

where  $B = 10^{12} B_{12}$  G,  $P_0$  is the initial pulsar period in seconds, and we have used  $R = 1.2 \times 10^6$  cm and  $I = 1.4 \times 10^{45}$  g cm<sup>2</sup>. Note that Eq. 15 neglects other sources

of loss of rotational kinetic energy, e.g. by gravitational radiation or electromagnetic quadrupole radiation (see the discussion by Manchester and Taylor [38]). The electromagnetic quadrupole radiation which might be important in very young pulsars is very uncertain and we shall neglect this. However, gravitational radiation losses are known to be important for very young pulsars and the power in gravitational radiation ( $\text{erg s}^{-1}$ ) is given by

$$L_{\text{gr}}(\Omega, k) = -\frac{32 G_N}{5} \frac{I^2 k^2 \Omega^6}{c^5} \quad (16)$$

where  $G_N$  is the gravitational constant,  $I$  is the moment of inertia and  $k$  is the ellipticity [37]. We adopt  $k = 3 \times 10^{-4}$  which is required in the case of the Crab pulsar to give a pulsar age equal to the time elapsed since the observation of the Crab supernova in AD 1054 [37].

Starting with an initial pulsar period we have performed numerical integrations over pulsar age to obtain the period as a function of age for the case where both electromagnetic losses and gravitational radiation losses are included. We show in Fig. 3 the period as a function of age for  $B \sin i = 10^{12}$  G and  $k = 3 \times 10^{-4}$  for two initial periods:  $P_0 = 5$  ms and  $P_0 = 10$  ms.

According to standard models of neutron star cooling, the surface temperature decreases to  $T_s \sim 10^7$  K at a few days after the explosion, and later cools much more slowly, reaching  $T_s \sim 4 \times 10^6$  K in one year. In our calculations, we interpolate/extrapolate the results of Nomoto and Tsuruta [24] for which  $\log(T_s/1 \text{ K})$  is 6.99, 6.72, 6.58, and 6.55 at  $\log(t/1 \text{ y}) = -2, -0.94, 0.08,$  and 1.11 respectively.

Models of high energy processes in pulsars predict polar cap temperatures can be significantly higher because of the heating caused the relativistic  $e^\pm$  pairs and  $\gamma$ -rays created in the gaps in the pulsar magnetosphere. For the space charge limited flow model [27, 42, 43] a lower limit on the polar cap temperature can be estimated

$$T_c^{AS} \approx 2.6 \times 10^5 P^{-19/32} B_{12}^{1/4} R_6^{5/16} \quad \text{K}, \quad (17)$$

where  $P$  is in seconds and  $R = 10^6 R_6$  cm. In deriving this formula it is assumed that the heating rate (given by Eq. 75 in Arons & Scharlemann [27]) applies to the region of the polar cap defined by the last open field line which intersects the pulsar surface at  $(r, \theta) = (R, \theta_c)$  where

$$\theta_c \approx (\Omega R/c)^{1/2} \quad (18)$$

giving a polar cap radius of

$$r_c \approx (2\pi R^3/cP)^{1/2}. \quad (19)$$

Arons & Scharlemann [27] note that the heating rate may actually be even higher, as given by the model of Ruderman & Sutherland [26], if most of the electrons from  $e^\pm$  pairs

created in the polar gap can be reversed and fall on the polar cap region. The Ruderman & Sutherland heating rate (given by Eq. 26 in their paper) defines an upper limit to the polar cap temperature

$$T_c^{RS} \approx 2.8 \times 10^6 P^{-8/28} B_{12}^{6/28} R_6^{-17/28} \text{ K}. \quad (20)$$

Note that in both models the polar cap temperatures depends on the pulsar parameters. For very rapid pulsars with high magnetic fields they can reach  $\sim 10^7$  K or higher. In the present paper we shall consider three cases: (1) no polar cap heating (the whole star has temperature  $T_s$ ); (2) surface except for polar cap has temperature  $T_s$  and polar cap has the higher of  $T_s$  or  $T_c^{AS}$  (Eq. 17) referred to as “moderate polar cap heating”; and (3) surface except for polar cap has temperature  $T_s$  and polar cap has the higher of  $T_s$  or  $T_c^{RS}$  (Eq. 20) referred to as “maximum polar cap heating”.

For hot polar caps, thermionic emission of ions is allowed, and because of the free supply of charges from the polar caps, the rotation-induced potential should be space charge limited (e.g. refs. [27, 39, 40]). Whether ions or electrons are accelerated out along field lines depends on the sign of the accelerating electric field. Here we consider only the case in which ions are accelerated.

It is usually assumed that the pulsar surface is composed largely of highly ionized Fe although other compositions, e.g. He nuclei [41], are also possible. Here, we assume that the all the outflowing ions are fully-ionized Fe (e.g. [40]). Fe nuclei accelerated in the magnetosphere may reach sufficiently high Lorentz factors such that photodisintegration could occur efficiently. To gain an impression about the pulsar parameters for which this may be important, we assume particles are accelerated by the electric field in the slot gap [27, 42, 43]. In this model the electric potential in the gap is given approximately by

$$\Phi(x) \approx 1.13 \times 10^2 \theta_c^4 B R g(x) \eta (1 - \eta^2) \sin \zeta \sin i \text{ V}, \quad (21)$$

where  $\eta$  is the ratio of the colatitude angle of the open field lines at the surface to  $\theta_c$ , and  $\zeta$  is the azimuthal angle with respect to the magnetic pole. In the equation,  $g(x) \approx x^2$  for  $x < 0.5\theta_c$ , and  $g(x) \approx \theta_c [(x + 1)^{0.5} - 1]$  for  $x > 0.5\theta_c$ , and  $x$  is the distance along the gap in units of  $R$ . In writing Eq. 21, we ignore the terms due to the complicated geometry of the gap. The ion acceleration zone corresponds to  $i > \pi/2$ . We shall adopt  $\eta = 0.1$  and  $\zeta = 3\pi/2$  in our work. This potential is shown in Fig. 4 for  $B \sin i = 10^{12}$  G and for periods equal to the two initial periods, i.e.  $P = 5$  ms and  $P = 10$  ms.

## 5 Spectrum of neutrons from photodisintegration of Fe nuclei

The extraction of energetic neutrons from accelerated nuclei has important consequences for the transport of energy from the pulsar’s vicinity to the nebula since they move ballistically through the magnetosphere and beyond the light cylinder. Their Lorentz factors



are approximately equal to the Lorentz factors of the parent nuclei, and are sufficiently high that they typically decay at large distances from the pulsar. Initially the SNR shell is opaque to neutrons so that most neutrons interact in the dense shell. Later, when the shell becomes more transparent to neutrons, they typically move through the SNR shell and decay outside it. Most of the energy of the neutrons is then taken by protons which are trapped and isotropized by the ambient magnetic field, and these protons then wait for target nuclei, i.e. the SNR shell, to arrive. When the SNR shell catches up with the relativistic protons, production of  $\gamma$ -rays and neutrinos occurs through hadronic collisions but, as we shall discuss in Section 6, this contribution is negligible for the present radiation field and electric potential. The protons will also contribute to the Galactic cosmic rays, although their contribution is relatively small.

The dependence of the electric potential in the case of the slot gap model as a function of distance (Eq. 21) defines the Lorentz factor of Fe nuclei during their propagation from the surface. Using this potential we compute the average number of neutrons extracted from Fe nuclei as a function of pulsar age. We show this in Fig. 5(a) for  $P_0 = 5$  ms for each of the three radiation field models: no polar cap heating, moderate polar cap heating, and maximum polar cap heating. Note that with maximum polar cap heating the polar cap temperature is not significantly higher than the stellar surface for  $t < 2.2$  days, and with moderate polar cap heating the polar cap temperature is not significantly higher than the stellar surface for  $t < 18$  days. In Fig. 5(b) we show the average cumulative number of neutrons extracted from a single Fe-nucleus during acceleration for  $P = 5$  ms as a function of distance along the slot gap for the three radiation field models.

Since at a particular distance, a neutron extracted from the accelerated ion will have an energy determined by the slot gap potential, we can now compute the energy spectra of neutrons escaping from the pulsar radiation field per single Fe nucleus accelerated. In Fig. 6 we show the spectrum of neutrons extracted from a single Fe-nucleus during acceleration,  $N_n(E_n)$ , for a pulsar with  $P_0 = 5$  ms and  $B \sin i = 10^{12}$  G, for the three radiation field models. Results are given for (a)  $t = 1.15$  days ( $P = 5$  ms), (b)  $t = 20.5$  days ( $P = 5.05$  ms), and (c)  $t = 1$  year ( $P = 5.69$  ms). In Fig. 7 we compare the spectrum of neutrons at  $t = 1$  year produced for  $P_0 = 5$  ms with that produced with  $P_0 = 10$  ms.

The differential production rate,  $\dot{N}_n(E_n)$ , of neutrons extracted from Fe nuclei depends on the total rate of Fe nuclei injected,  $\dot{N}_{\text{Fe}}$ , and is given by

$$\dot{N}_n(E_n) = \dot{N}_{\text{Fe}} N_n(E_n) = \frac{\xi L_{\text{em}}(\Omega, B)}{Ze\Phi_{\text{max}}(\Omega, B)} N_n(E_n) \quad (22)$$

where  $L_{\text{em}}(\Omega, B)$  is the magnetic dipole radiation approximation to the total non-gravitational radiation spin-down power (Eq. 14),  $\Phi_{\text{max}}(\Omega, B) = \Phi(r_{\text{LC}}/R)$  is the maximum acceleration potential traversed by Fe nuclei given by Eq. 21 and  $r_{\text{LC}}$  is the distance to the light cylinder up to which this acceleration is assumed to occur,  $Z = 26$  is the atomic number of Fe, and  $e$  unit electric charge. The parameter  $\xi$  gives the fraction of total pulsar power used to accelerate Fe nuclei and has an upper-limit  $\xi \approx \Phi_{\text{max}}/\Phi_0 \approx 0.29$  where  $\Phi_0 = 0.5\theta_c^4 BR$

is the maximum potential drop across the polar cap (e.g. Luo et al. [44]). Note that we write the rate of injection of iron nuclei as the ratio of a fraction of the power,  $\xi L_{\text{em}}$  to the maximum particle energy,  $Ze\Phi_{\text{max}}$  since the ratio gives the same order-magnitude estimate of the injection rate as that derived from Goldreich-Julian density.

## 6 Gamma-ray and neutrino spectra

We make the approximation that in shell-type SNR the shell has a thickness which is much smaller than the radius of the shell,  $r_{\text{SN}}$ . The optical depth of the shell to nucleon-nucleon collisions is then

$$\tau_{pp} = M_{\text{SN}}\sigma_{pp}/(4\pi r_{\text{SN}}^2 m_p) \approx 3.5 \times 10^{-5} M_{10}/(\beta_{\text{SN}} t_y)^2 \quad (23)$$

where  $M_{\text{SN}} = 10M_{10} M_{\odot}$  is the mass ejected into the shell during the explosion,  $\sigma_{pp} \approx 3 \times 10^{-26} \text{ cm}^2$  is the proton-proton inelastic cross section,  $m_p$  is the proton mass,  $t = t_y$  years is the time after the explosion, and  $v_{\text{SN}} = \beta_{\text{SN}}c$  is the shell expansion velocity. Initially the shell is optically thick. For example, if  $M_{\text{SN}} = 10M_{\odot}$  and  $\beta_{\text{SN}} = 0.03$  the optical depth is greater than 1 for  $t < 2$  months. All the results we shall present below are for  $\beta_{\text{SN}} = 0.03$  and  $M_{\text{SN}} = 10 M_{\odot}$ .

During the early phase most of the neutrons interact with matter in the shell producing  $\gamma$ -ray and neutrino fluxes. These signals may be observed provided the  $\gamma$ -ray and neutrino beams intersect the direction to the Earth, or sweep across the Earth giving rise to a pulsed signal. For a beaming solid angle of  $\Omega_b$  steradians, the neutrino flux may be calculated from

$$F_{\nu}(E_{\nu}) \approx \frac{\dot{N}_{\text{Fe}}}{\Omega_b d^2} [1 - \exp(-\tau_{pp})] \int N_n(E_n) P_{n\nu}^M(E_{\nu}, E_n) dE_n \quad (24)$$

where  $d$  is the distance to the SNR, and  $P_{n\nu}^M(E_{\nu}, E_n)dE_{\nu}$  is the number of neutrinos produced with energies in the range  $E_{\nu}$  to  $(E_{\nu} + dE_{\nu})$  (via pion production and subsequent decays) in multiple nucleon-nucleon interactions of a nucleon of energy  $E_n$ . Nucleon-nucleon interactions were treated as described in [45] and the pions produced were decayed using SIBYLL [46]. All the results given below are for  $\Omega_b = 1 \text{ sr}$ , and for smaller beams the fluxes should therefore be scaled up by a factor  $\Omega_b^{-1}$ .

In the case of  $\gamma$ -ray production, a significant fraction of the  $\gamma$ -rays will interact by pair production with target nuclei in the shell and will not be observed. Also, during the first few months, TeV  $\gamma$ -rays could interact with radiation from the photosphere of the supernova [47]. By several days after the explosion, the radius of the photosphere becomes smaller than that of the SNR shell, where the neutrons interact, and continues to decrease in radius relative to the shell. Thus, interactions with radiation from the photosphere is likely to be a small effect here as the  $\gamma$ -rays will be traveling in the directions of their parent neutrons, i.e. radially outwards from the neutron star, and the angle between the directions of the  $\gamma$ -rays and soft photons from the photosphere will be small, reducing

the interaction probability. Concentrating on pair production with matter, the optical depth of the shell is determined by the mean free path for pair production which at high energies is  $(9/7)$  of the radiation length, giving  $\tau_{\gamma p} \approx 0.7\tau_{pp}$ . For a neutron interacting at some fraction,  $f$ , of the way through the shell, a  $\gamma$ -ray produced at that point would have a probability of  $\exp[-(1-f)\tau_{\gamma p}]$  of escaping from the shell. Integrating over neutron interaction points ( $\gamma$ -ray emission points) within the shell we arrive at the gamma ray flux at Earth,

$$F_{\gamma}(E_{\gamma}) \approx \frac{\dot{N}_{\text{Fe}}}{\Omega_b d^2} \frac{\exp(-\tau_{pp}) - \exp(-\tau_{\gamma p})}{(\tau_{\gamma p}/\tau_{pp}) - 1} \int N_n(E_n) P_{n\gamma}^M(E_{\gamma}, E_n) dE_n, \quad (25)$$

where  $P_{n\gamma}^M(E_{\gamma}, E_n)dE_{\gamma}$  is the number of  $\gamma$ -rays produced with energies in the range  $E_{\gamma}$  to  $(E_{\gamma} + dE_{\gamma})$  (via pion production and subsequent decays) by multiple nucleon-nucleon interactions of a nucleon of energy  $E_n$ . Note that this neglects cascading in the matter as a result of bremsstrahlung and subsequent pair production, and so the  $\gamma$ -ray flux at low energies will be somewhat underestimated.

Light curves for neutrinos above 1 TeV, and  $\gamma$ -rays above 100 MeV and 1 TeV, are shown for  $B \sin i = 10^{12}$  G in Fig. 8(a) for  $P_0 = 5$  ms and in Fig. 8(b) for  $P_0 = 10$  ms. The results are shown here, and in the remaining figures, for a distance of  $d = 10$  kpc. In both cases, results are given for three radiation field models (no polar cap heating, moderate polar cap heating, and maximum polar cap heating), and the pulsar period and the surface and polar cap temperatures vary appropriately with time after the explosion. In Fig. 9(a) we show the energy spectrum of  $\gamma$ -rays, and in Fig. 9(b) the energy spectrum of neutrinos, both at  $t = 0.1$  year for each initial period and radiation field model. In Fig. 10 we show how the energy spectrum of neutrinos evolves with time for the case of  $P_0 = 5$  ms and the maximum polar cap heating model. In both Figs. 9(b) and 10 we show the atmospheric neutrino background flux within  $1^\circ$  and within  $10^\circ$  of the source direction based on the intensity calculated by Lipari [48].

## 7 Discussion and Conclusion

As we shall see, we require fairly high acceleration efficiencies in very young pulsars for observable fluxes of  $\gamma$ -rays and neutrinos. However, high energy  $\gamma$ -ray observations of several pulsars appear to suggest an increase in  $\gamma$ -ray efficiency with age. This may be attributed to the relation between acceleration efficiency for primary particles that start the electron-positron pair cascade and the age, provided the pulsed  $\gamma$ -ray emission from pulsars is from pair cascades. This may be true for young pulsars with ages more than  $\sim 10^3$  years. For *very* young pulsars (a few months to a few years) as discussed in this paper, thermal emission from the polar caps or neutron star's surface may have an important effect on particle acceleration. For very young pulsars with strong magnetic fields and hot polar caps, the efficiency may be higher for younger pulsars. This is because energy losses due to resonant inverse Compton scattering are important and can prevent primary electrons or positrons from starting a cascade in regions near the polar caps [49].

We next discuss whether the signals we predict from young SNR are observable with existing and planned experiments (see e.g. ref. [50] for a summary of  $\gamma$ -ray detector thresholds). The  $\gamma$ -ray light curve peaks at about 2 months after the explosion (see Fig. 8). The peak flux above 100 MeV for a pulsar at 10 kpc with  $B \sin i = 10^{12}$  G ranges from  $2 \times 10^{-10} \text{ cm}^{-2} \text{ s}^{-1}$  ( $P_0 = 10$  ms, no polar cap heating) to  $4 \times 10^{-9} \text{ cm}^{-2} \text{ s}^{-1}$  ( $P_0 = 5$  ms, maximum polar cap heating) if  $\xi \Omega_b^{-1} = 1 \text{ sr}^{-1}$ . The sensitivity of the EGRET detector on the Compton Gamma Ray Observatory for 100 MeV  $\gamma$ -rays is  $\sim 7 \times 10^{-8} \text{ cm}^{-2} \text{ s}^{-1}$ , and with this sensitivity  $\gamma$ -rays from a Galactic source should easily be detected for several months if a significant fraction of the electromagnetic power ( $\xi \sim 1$ ) goes into accelerating heavy nuclei and the pulsar's  $\gamma$ -ray beam sweeps across the Earth and has  $\Omega_b < 0.07 \text{ sr}$  ( $P_0 = 5$  ms, maximum polar cap heating) or  $\Omega_b < 3 \times 10^{-3} \text{ sr}$  ( $P_0 = 10$  ms, no polar cap heating). With future 100 MeV  $\gamma$ -ray detectors, even lower detection thresholds (e.g.  $\sim 5 \times 10^{-9} \text{ cm}^{-2} \text{ s}^{-1}$  for GLAST) should enable detection even if  $\Omega_b$  were larger.

The current generation of Cherenkov telescopes operating at TeV energies (e.g. the Whipple Observatory, and the CANGAROO telescope [51]) have thresholds of a  $\sim 3 \times 10^{-12} \text{ cm}^{-2} \text{ s}^{-1}$ , and GRANITE III (Whipple telescope with new camera) is expected to have a threshold of  $\sim 10^{-12} \text{ cm}^{-2} \text{ s}^{-1}$ . For Galactic sources, the predicted TeV fluxes (see Fig. 8) are well above the Whipple threshold and should easily be detected even for the least optimistic case ( $P_0 = 10$  ms, no polar cap heating) provided  $\xi^{-1} \Omega_b < 3.8 \text{ sr}$ , for the most optimistic case ( $P_0 = 5$  ms, maximum polar cap heating) provided  $\xi^{-1} \Omega_b < 75 \text{ sr}$ . With the sensitivity of current TeV  $\gamma$ -ray telescopes, it should be possible to detect  $\gamma$ -rays from sources in the Magellanic Clouds provided  $\xi^{-1} \Omega_b$  is sufficiently high, and we shall discuss below constraints placed on our model by the non-detection of  $\gamma$ -rays from SN 1987A.

Available upper limits on the TeV  $\gamma$ -ray flux from SN 1987A are as follows:  $t \approx 10$  months (November 1987) —  $2.3 \times 10^{-11} \text{ cm}^{-2} \text{ s}^{-1}$  above 1 TeV (Raubenheimer et al. [12]);  $t \approx 1$  year —  $6.1 \times 10^{-12} \text{ cm}^{-2}$  above 3 TeV (Bond et al. [8]);  $t \approx 1$  year (January/February 1988) —  $1.6 \times 10^{-10} \text{ cm}^{-2} \text{ s}^{-1}$  above 0.4 TeV (Chadwick et al. [10]). Assuming a distance of 55 kpc, and if the observer is inside the beam of energetic neutrons injected by the pulsar, which will also define the  $\gamma$ -ray beam, then the value of  $\xi^{-1} \Omega_b$  can be constrained by the 1 TeV upper limit mentioned above, giving  $\xi^{-1} \Omega_b > 0.36 \text{ sr}$  for the case of  $P_0 = 5$  ms (see Fig. 8a). However, we note that since no pulsar has yet been discovered inside SN 1987A this could be interpreted as suggesting that we are outside the beam of the neutron injection or that no pulsar was formed.

The technique for constructing a large area (in excess of  $10^4 \text{ m}^2$ ) neutrino telescope has been known for more than a decade [52]. In pioneering work, the DUMAND Collaboration developed techniques to instrument a large volume of water in a deep ocean trench with strings of photomultipliers to detect Cherenkov light from neutrino-induced muons. Locations deep in the ocean shield the detectors from cosmic ray muons. The DUMAND detector [53] was designed to be most sensitive to neutrinos above about 1 TeV, and prototypes of other similar experiments are already in operation such as that in Lake Baikal, Siberia [54], and NESTOR off the coast of Greece [55]. An exciting recent

development has been the construction of a DUMAND type detector deep in the polar ice cap at the South Pole. This experiment called AMANDA uses the same principle as DUMAND but takes advantage of excellent transparency of the polar ice under extreme pressures and a stable environment in which to embed the detectors [56]. These experiments which operate typically above 1 TeV have the potential to be expanded in the future to a detector on the 1 km<sup>3</sup> scale. The background to these experiments at 1 TeV is due primarily to atmospheric neutrinos, but at higher energies there is an uncertain background of prompt muons from charm production (see e.g. Gaisser et al. [57] for a discussion). For recent reviews of the predicted intensity of diffuse high energy neutrinos of astrophysical origin see refs. [57, 58].

Referring to Figs. 9(b) and 10 we see that for good angular resolution (1°) the neutrino flux above 1 TeV is well above the atmospheric background, and even for 10° resolution the neutrino signal may be observable. However, observation of any signal would require the neutrino beam (essentially the beam of the primary neutrons) to sweep across the Earth. For 1° resolution and  $\xi\Omega_b^{-1} = 1 \text{ sr}^{-1}$ , TeV neutrinos should be easily observable if their flux remained constant at the level given in Fig. 9(b) for 0.1 y. However, the neutrino light curve drops rapidly at  $t > 0.1 \text{ y}$  (see Fig. 8(b)) and so very large neutrino telescopes will be required. With 10° resolution, detection of galactic sources at 1 TeV would be marginal even in the most optimistic scenario except for the case of extremely large detectors, e.g. km<sup>3</sup> [59] which, with large statistics, could see a weak signal significantly below the atmospheric background. Note, however, that the emission peaks at energies  $\sim 10\text{--}100 \text{ TeV}$ , and that telescopes sensitive in this range should be able to detect a neutrino signal for the  $P_0 = 5 \text{ ms}$  case from a galactic source even if the resolution were 10°. A large detector with excellent angular resolution would be required to observe very young SNR in the Magellanic Clouds unless the emission were beamed strongly towards the Earth.

We have neglected any signals arising from the protons extracted from Fe-nuclei, and also signals from nuclei that were not completely fragmented into nucleons in the radiation field of the pulsar. We assume these particles, being charged, will be trapped in the central region of the SNR where the matter density is expected to be relatively low, and would not contribute significantly to the  $\gamma$ -ray and neutrino fluxes. These nuclei would be subject to adiabatic deceleration as the SNR expands. However, some would accumulate and eventually contribute to the galactic cosmic rays towards the end of the SNR's life. Neutrons that do not interact promptly travel far from the pulsar where they decay into protons which await the arrival of target nuclei in the supernova shell, and then produce a delayed isotropic neutrino and  $\gamma$ -ray signal. We have estimated these delayed neutrino and  $\gamma$ -ray fluxes for the present radiation field models and slot gap potential. The  $\gamma$ -ray light curves peak at about 6 months with fluxes about  $10^{-3}$  of the peak flux from neutron collisions in the shell for  $\Omega_b = 1 \text{ sr}$ . Thus, unlike the case of  $\gamma$ -rays from interactions of neutrons with the shell, the delayed fluxes are unlikely to be observable. The TeV neutrino light curve is of the same magnitude as the TeV  $\gamma$ -ray light curve. Those protons from neutron decay outside the nebula also contribute to the Galactic cosmic rays. We estimate

the total energy going into cosmic rays, with typical energies of  $10^6$  GeV, integrated over the pulsar's age to be  $\sim 10^{45}$  erg, which is much less than the  $\sim 10^{50}$  erg potentially available through shock acceleration.

In the case of filled nebulae, the  $\gamma$ -ray and neutrino fluxes could be higher than estimated here. For example,  $\tau_{pp}$  would be a factor of 3 higher than given by Eq. 23 in the case of uniform filling. More importantly, cosmic rays trapped inside the nebula would also continuously contribute to the  $\gamma$ -ray and neutrino fluxes. Such a model is discussed in the context of the Crab Nebula in another paper [31].

We have investigated the use of higher magnetic fields, e.g  $10^{13}$  G, and found that this has two main effects: (1) the polar cap heating is increased resulting in more neutrons extracted per Fe nucleus (but up to a maximum of 30), (2) the maximum acceleration potential is increased. The second effect causes the peak of the  $\gamma$ -ray and neutrino emission to move to higher energies, and the injection rate of Fe nuclei to decrease (see Eq. 22). Overall, the net effect of using extremely high magnetic fields is unexpectedly to reduce the predicted fluxes to levels comparable to or lower than those predicted here for typical pulsar magnetic fields.

We should point out that in this paper we have ignored the fall-back of matter onto the neutron star. If fall-back occurs, which cannot be ruled out, there are two immediate consequences: acceleration of lighter ions such as carbon nuclei may occur, or acceleration is completely quenched. In the present work we have also ignored production of  $\gamma$ -ray lines. The neutrons and protons from the Fe photodisintegration will excite nuclei of C, N, O, etc. in the supernova shell to make gamma-ray lines in the 1–10 MeV range. These lines may be detectable after about 1 year, when the shell becomes optically thin to scattering and absorption. Calculation of the flux of these lines is however beyond the scope of the present paper.

In Conclusion, we have considered a model for  $\gamma$ -ray and neutrino emission by very young supernova remnants in which ions are accelerated in the slot gap of a highly magnetized rapidly spinning pulsar. Energetic neutrons are extracted from the ions by photodisintegration during interactions with thermal radiation from the neutron star surface and hot polar caps. Gamma ray and neutrino signals are produced by energetic neutrons interacting with target nuclei as they travel out through the SNR shell. For a limited range of pulsar parameters these signals should be observable from very young SNR in our Galaxy with existing and planned  $\gamma$ -ray and neutrino telescopes within one or two years of the supernova explosion. The emission peaks above TeV energies and so ground-based optical Cherenkov detectors are more sensitive than the lower energy satellite telescopes. Neutrino telescopes should also be able to detect the predicted neutrino signals which peak at  $\sim 10$  TeV energies.

## Acknowledgements

We thank Jörg Rachen for suggesting the use of the Weizaeker-Williams method when considering photodisintegration by a magnetic field. W.B. thanks the Department of Physics

and Mathematical Physics at the University of Adelaide for hospitality during his visit. Q.L. acknowledges receipt of an Australian Research Council (ARC) Postdoctoral Fellowship. This research is supported by a grant from the ARC.

## References

- [1] Berezhinsky, V.S., and Prilutsky, O.F., *Astron. Astrophys.* **66** (1978) 325.
- [2] Sato, H., *Prog. Theor. Phys.* **58** (1978) 549.
- [3] Gaisser, T.K., Harding, A.K., Stanev, T., *Nature* **329** (1987) 314.
- [4] Gaisser, T.K., Harding, A.K., and Stanev, T., *Ap.J.* **345** (1989) 423.
- [5] Yamada, Y., Nakamura, T., Kasahara, K., and Sato, H., *Prog. Theor. Phys.* **79** (1987) 426.
- [6] Berezhinsky, V.S., and Ptuskin, V.S., *Astron. Astrophys.* **215** (1989) 339.
- [7] Bond, I.A. et al. *Phys. Rev. Lett.* **60** (1988) 1110.
- [8] Bond, I.A. et al. *Phys. Rev. Lett.* **61** (1988) 2292.
- [9] Bond, I.A. *Ap.J.* **344** (1989) L17.
- [10] Chadwick, P.M., et al. *Ap.J.* **333** (1988) L19.
- [11] Ciampa, D. et al. *Ap.J.* **326** (1988) L9.
- [12] Raubenheimer, B.C. et al. *Astron. Astrophys.* **193** (1988) L11.
- [13] Allen, W.H. et al. *Phys. Rev. D* **48** (1993) 466.
- [14] van Stekelenborg, J. et al. *Phys. Rev. D* **48** (1993) 4504.
- [15] Rees, M.J., Gunn, J.E., *Mon. Not. R. Astron. Soc.* **167** (1974) 1.
- [16] Berezhinsky, V.S., Ginzburg, V.L., *Nature* **329** (1987) 807.
- [17] Harding, A.K., Mastichiadis, A., Protheroe, R.J., Szabo, P., *Ap.J.* **378** (1991) 163.
- [18] Kirk, J.G., Duffy, P., Ball, L., *Astron. Astrophys.* **293** (1995) L37.
- [19] Hoshino, M., Arons, J., Gallant, Y.A., Langdon, A.B., *Ap.J.* **390** (1992) 454.
- [20] Gallant, Y.A., Arons, J., *Ap.J.* 435 (1994) 230.
- [21] Finley, J.P., Ögelman, H., Kiziloglu, Ü., *Ap.J.* **394** (1992) L21.

- [22] Halpern, J.P., Ruderman, M., *Ap.J.* **415** (1993) 286.
- [23] Ögelman, H., Finley, J.P., Zimmermann, H.U., *Nature* **361** (1993) 136.
- [24] Nomoto, K., Tsuruta, S., *Ap.J.* **312** (1987) 711.
- [25] Ögelman, H., *Neutron stars: Theory and Observation*, J. Ventura & D. Pines (eds.), (Kluwer), 87.
- [26] Ruderman, M., Sutherland, P.G. *Ap.J.* **196** (1975) 51.
- [27] Arons, J., Scharlemann, E.T., *Ap.J.* **231** (1979) 854.
- [28] Helfand, D.J., Chanan, G.A., Novick, R., *Nature* **283** (1980) 337.
- [29] Cheng, K.S., Ho, C., Ruderman, M., *Ap.J.* **300** (1986) 500
- [30] Cheng, K.S., Ho, C., Ruderman, M., *Ap.J.* **300** (1986) 522
- [31] Bednarek, W., and Protheroe, R.J., *Phys. Rev. Lett.* (1997) in press.
- [32] Bednarek, W., Karakuła, S., *Proc. 24th Int. Cos. Ray Conf.* (Rome) **2** (1995) 279.
- [33] Karakuła, S., Tkaczyk, W., *Astropart.Phys.* **1** (1993) 229.
- [34] Pavlov, G.G., Shibano, YU.A., Ventura, J., Zavlin, V.E., *Astron. Astrophys.*, **289** (1994) 837.
- [35] Jackson, J.D., “Classical Electrodynamics”, 2nd Ed., Wiley, New York, (1975).
- [36] De Jager, O.C., Nel, H.I., *Astron. Astrophys.*, **190** (1988) 87.
- [37] Shapiro, S.L., and Teukolsky, S.L., *Black Holes, White Dwarfs and Neutron Stars* (New York: Wiley, 1983).
- [38] Manchester, R.N., and Taylor, J.H, *Pulsars* (San Francisco: Freeman, 1977).
- [39] Michel, F. C., *Ap.J.* **192** (1974) 713.
- [40] Fawley, W. M., Arons, J. & Scharlemann, E. T., *Ap.J.* **217** (1977) 227.
- [41] Rosen, L. C. & Cameron, A. G. W., *Astroph. & Space Sci.* **15** (1972) 137.
- [42] Arons, J., *Ap.J.* **248** (1981) 1099.
- [43] Arons, J., *Ap.J.* **266** (1983) 215.
- [44] Luo, Q., Protheroe, R.J., & Bednarek, W., in preparation.
- [45] Hillas, A.H., in *Proc. 17th Int'l Cosmic Ray Conf.* (Paris, 1981) **8**, p. 193.



- [46] Fletcher R.S., Gaisser T.K., Lipari P., Stanev T. *Phys. Rev. D* **50** (1994) 5710.
- [47] Protheroe, R.J., *Nature* **329** (1987) 135.
- [48] Lipari, P., *Astroparticle Phys.* **1** (1993) 195.
- [49] Luo, Q., and Protheroe, R.J., *Publications of of the Astronomical Society of Australia*, submitted (1997)
- [50] Sembroski, G., et al., 24th Int. Cos. Ray Conf. (Rome) **3** (1995) 428
- [51] Hara, T., et al., Nuclear Instr. & Methods in Phys. Res. **A332** (1993) 300.
- [52] Berezhinskiĭ, V.S., and Zatsepin, G.T. *Sov. Phys. Usp.* **20** (1977) 361.
- [53] Learned, J.G., in “Frontiers of Neutrino Astrophysics”, eds. Y. Suzuki and K. Nakamura, (Universal Academy Press, Tokyo, 1993) p. 341.
- [54] Belolaptikov, I.A., *et al.*, in 24th Int. Cosmic Ray Conf. (Rome), **1** (1995) 742.
- [55] Capone, A., *et al.*, in 24th Int. Cosmic Ray Conf. (Rome), **1** (1995) 836.
- [56] Mock, P.C., *et al.*, in 24th Int. Cosmic Ray Conf. (Rome), **1** (1995) 758.
- [57] Gaisser, T.K., Halzen, F., and Stanev, T., *Phys. Rep.*, **258**, (1995) 173.
- [58] Protheroe, R.J., in *Towards the Millennium in Astrophysics: Problems and Prospects*, Erice 1996, eds. M.M. Shapiro and J.P. Wefel (World Scientific, Singapore), in press (1997) astro-ph/9612213
- [59] Halzen, F., Proc. Int. Symp. on Neutrino Telescopes, Venice, February 1996, in press, astro-ph/9605014

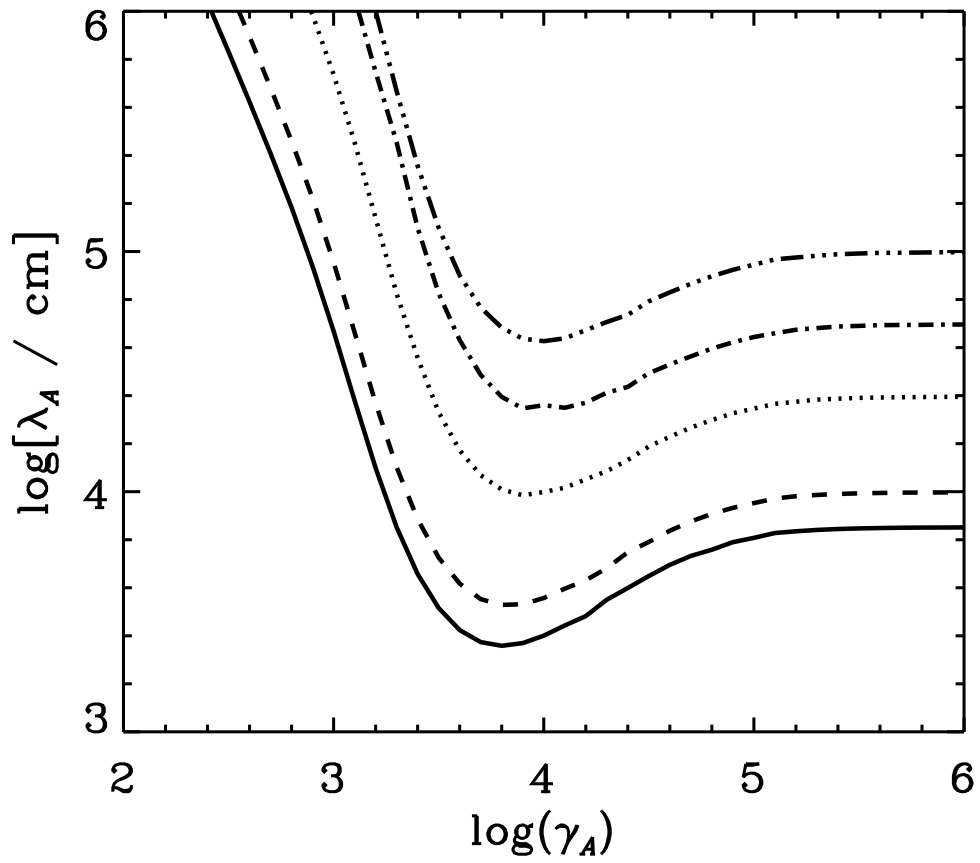


Figure 1: Mean free path for photodisintegration of nuclei in isotropic black body radiation at temperature  $T = 10^7$  K as a function of Lorentz factor,  $\gamma_A$ , for various mass numbers  $A$ : 4 (top curve), 8, 16, 40, and 56 (bottom curve).

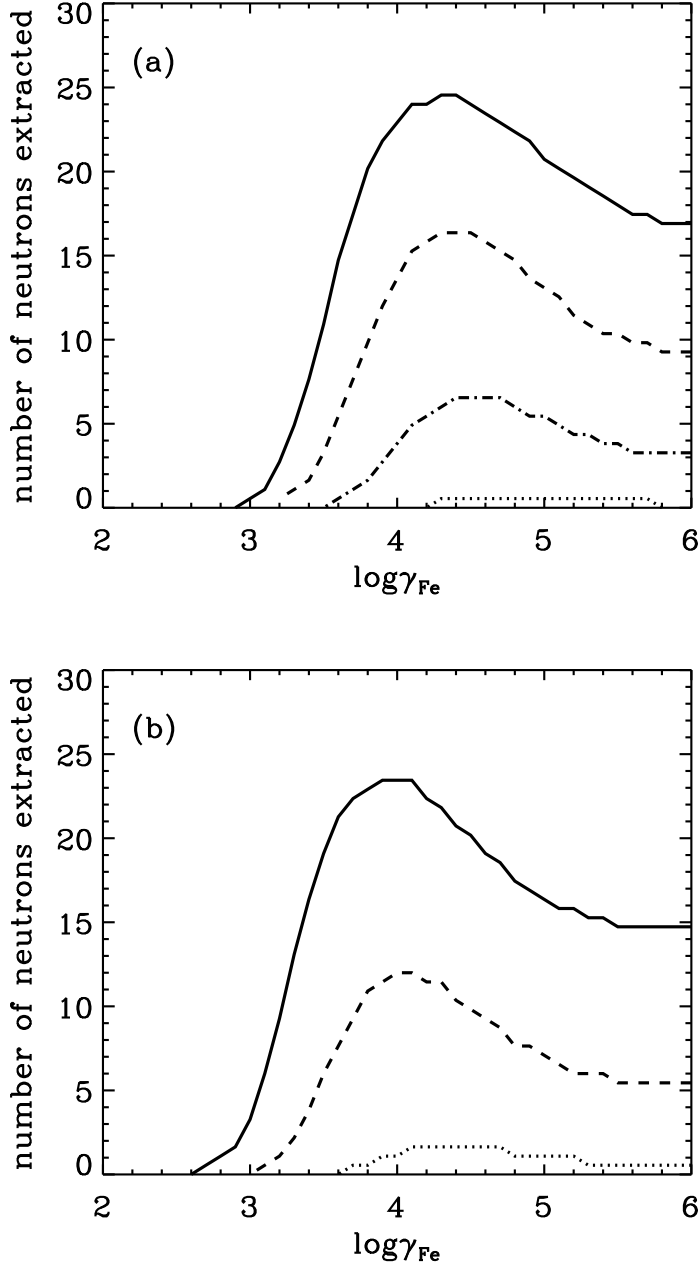


Figure 2: (a) Average number of neutrons extracted from a single Fe-nucleus during propagation along the neutron star’s magnetic axis, from its surface at the pole to infinity, as a function of Lorentz factor. Neutron star spherical surface of radius  $1.2 \times 10^6$  cm at constant temperature  $T = 5 \times 10^6$  K (bottom curve),  $10^7$  K,  $1.5 \times 10^7$  K, and  $2 \times 10^7$  K (top curve). (b) Average number of neutrons extracted from a single Fe-nucleus during propagation along the neutron star’s magnetic axis, from its surface at the pole to infinity, as a function of Lorentz factor, for field of heated polar cap of radius  $10^5$  cm with temperature  $T = 10^7$  K (bottom curve),  $2 \times 10^7$  K, and  $3 \times 10^7$  K (top curve).

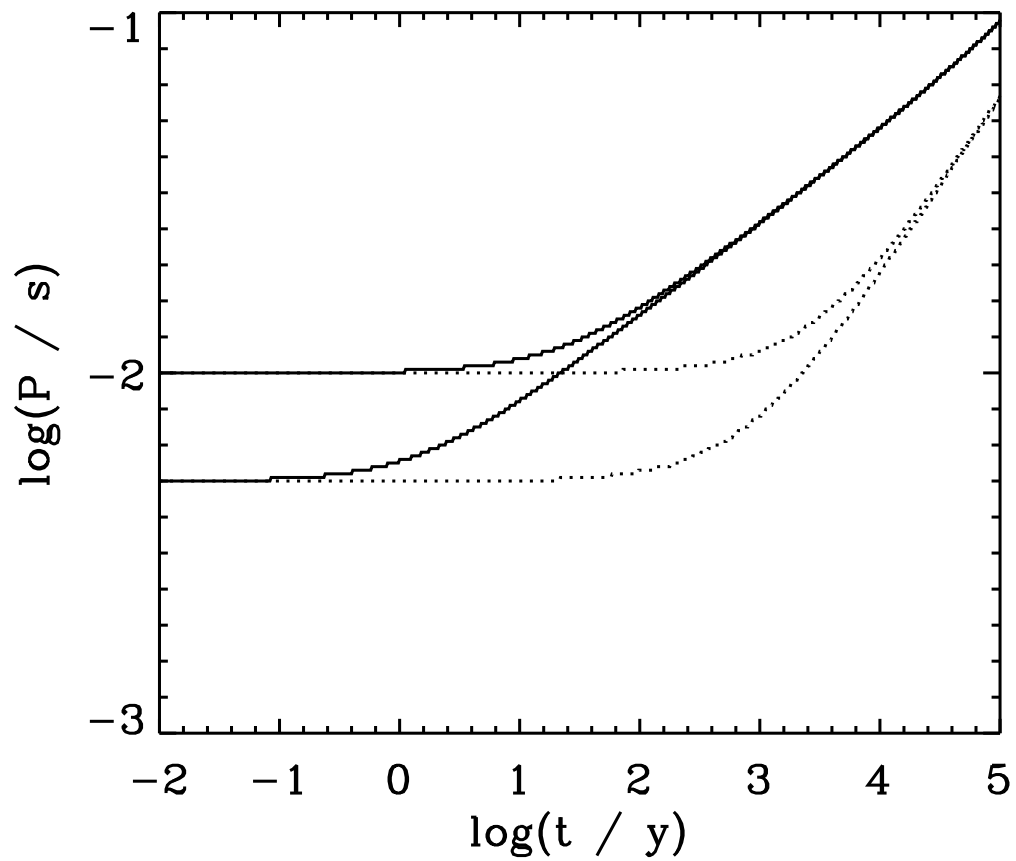


Figure 3: Evolution of pulsar period for  $B \sin i = 10^{12}$  G for  $P_0 = 5$  ms (lower curves) and  $P_0 = 10$  ms (upper curves). Dotted curves are for electromagnetic radiation losses only, and solid curves include the effect of gravitational radiation losses.

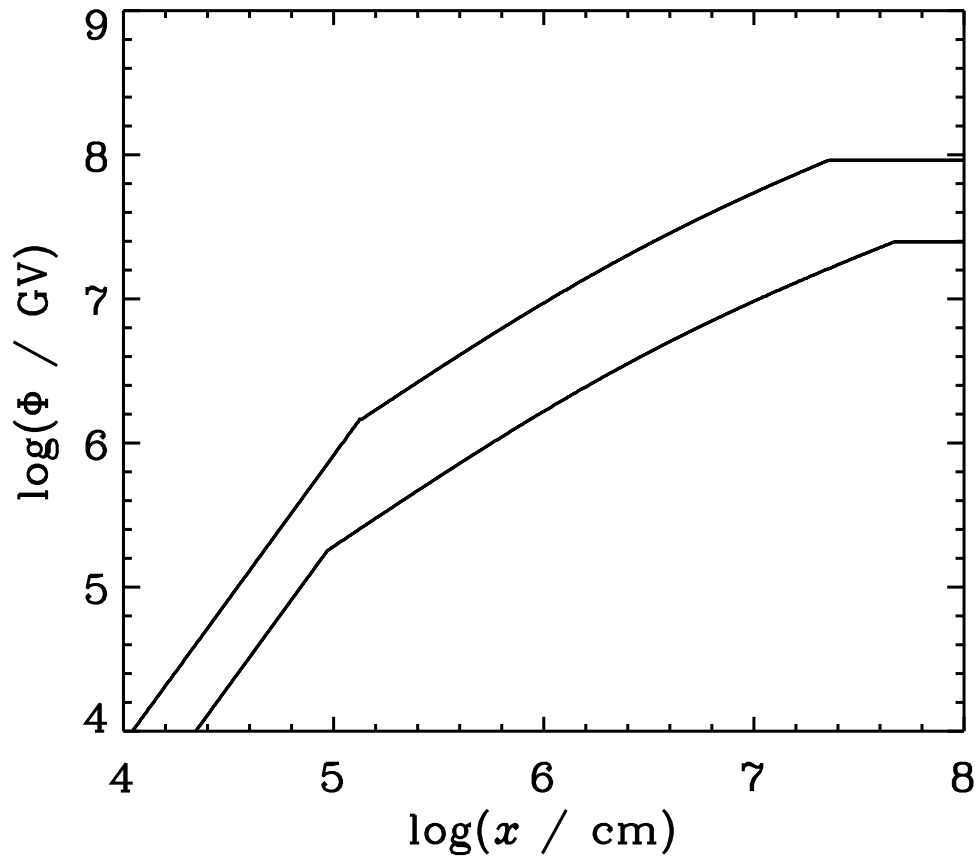


Figure 4: Slot gap potential given by Eq. 21 for  $B \sin i = 10^{12}$  G and  $P = 10$  ms (lower curve) and  $P = 5$  ms (upper curve). The potential is assumed constant for  $x$  larger than the light cylinder radius.

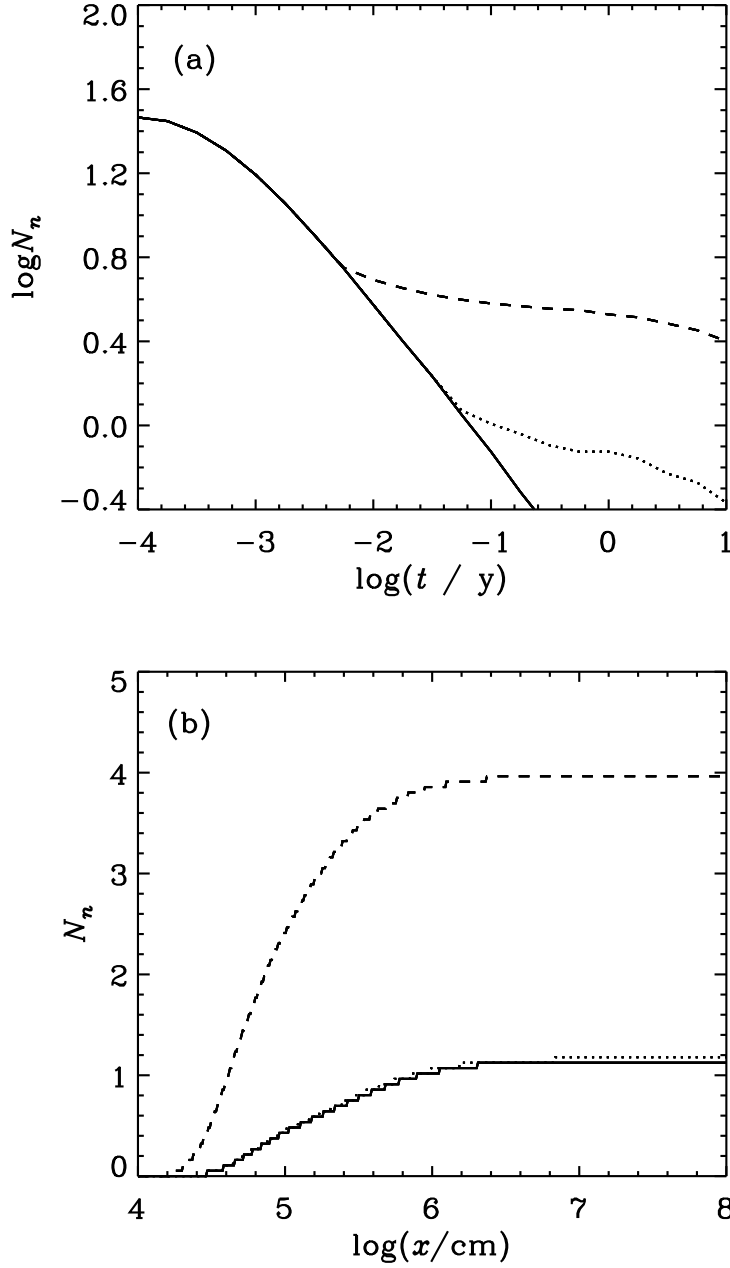


Figure 5: Average cumulative number of neutrons extracted from a single Fe-nucleus during acceleration by the assumed slot gap potential for  $B \sin i = 10^{12}$  G and  $P_0 = 5$  ms through the pulsar’s radiation field: (a) as a function of neutron star age; (b) as a function of distance along the slot gap at  $t = 20.5$  days. Results are shown for no polar cap heating (solid curve), moderate polar cap heating (dotted curve), and maximum polar cap heating (dashed curve).

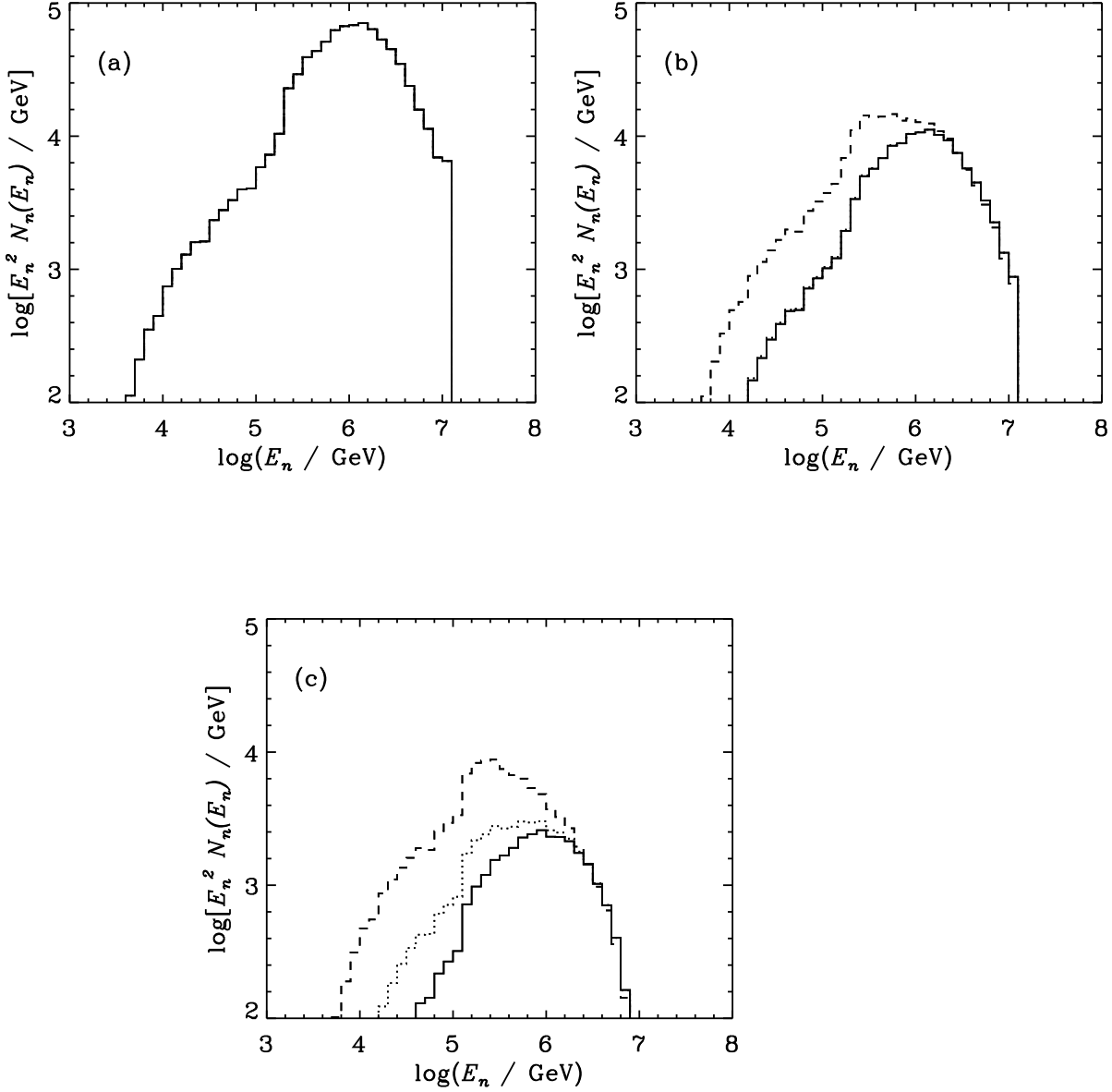


Figure 6: The spectrum of neutrons extracted from a single Fe-nucleus during acceleration for a pulsar with  $P_0 = 5$  ms and  $B \sin i = 10^{12}$  G at (a)  $t = 1.15$  days ( $P = 5.00$  ms), (b)  $t = 20.5$  days ( $P = 5.05$  ms), and (c)  $t = 1$  year ( $P = 5.69$  ms). Results are shown for the three radiation field models: no polar cap heating – solid histogram; moderate heating – dotted histogram; maximum heating – dashed histogram.

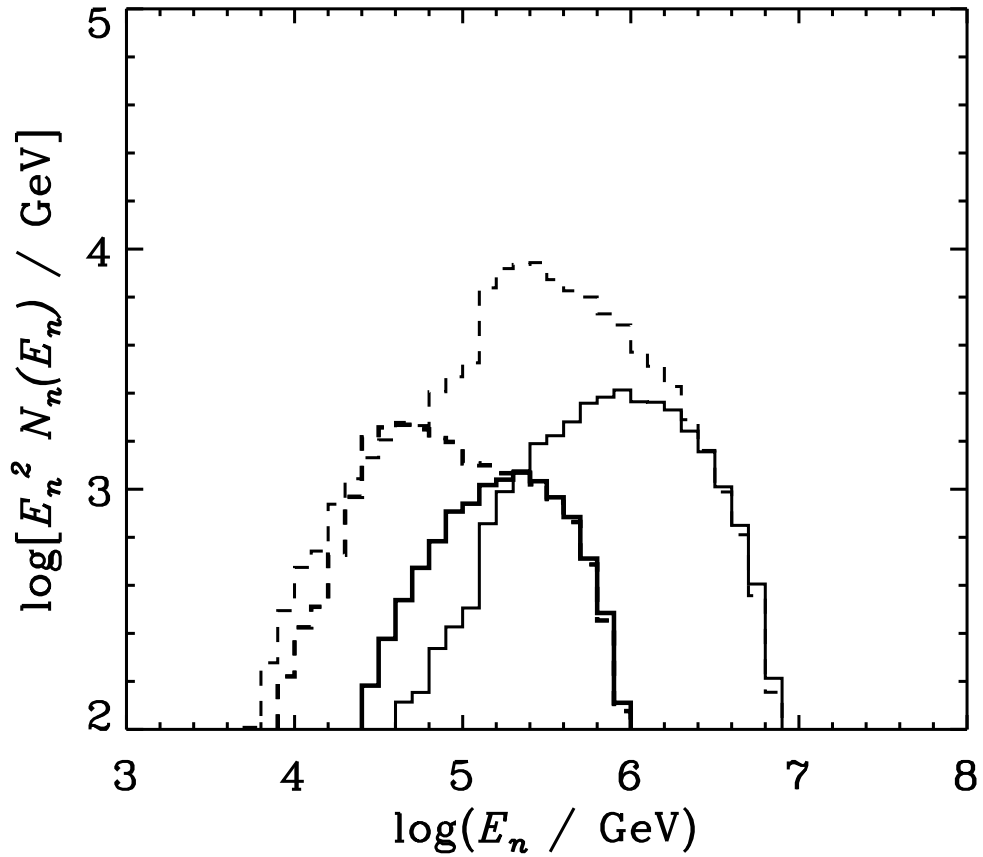


Figure 7: The spectrum of neutrons extracted from a single Fe-nucleus during acceleration at  $t = 1$  year and  $B \sin i = 10^{12}$  G for the following initial pulsar periods  $P_0 = 5$  ms (thin histograms), and  $P_0 = 10$  ms (thick histograms). Results are shown for two of the radiation field models: no polar cap heating – solid histograms; maximum heating – dashed histograms.



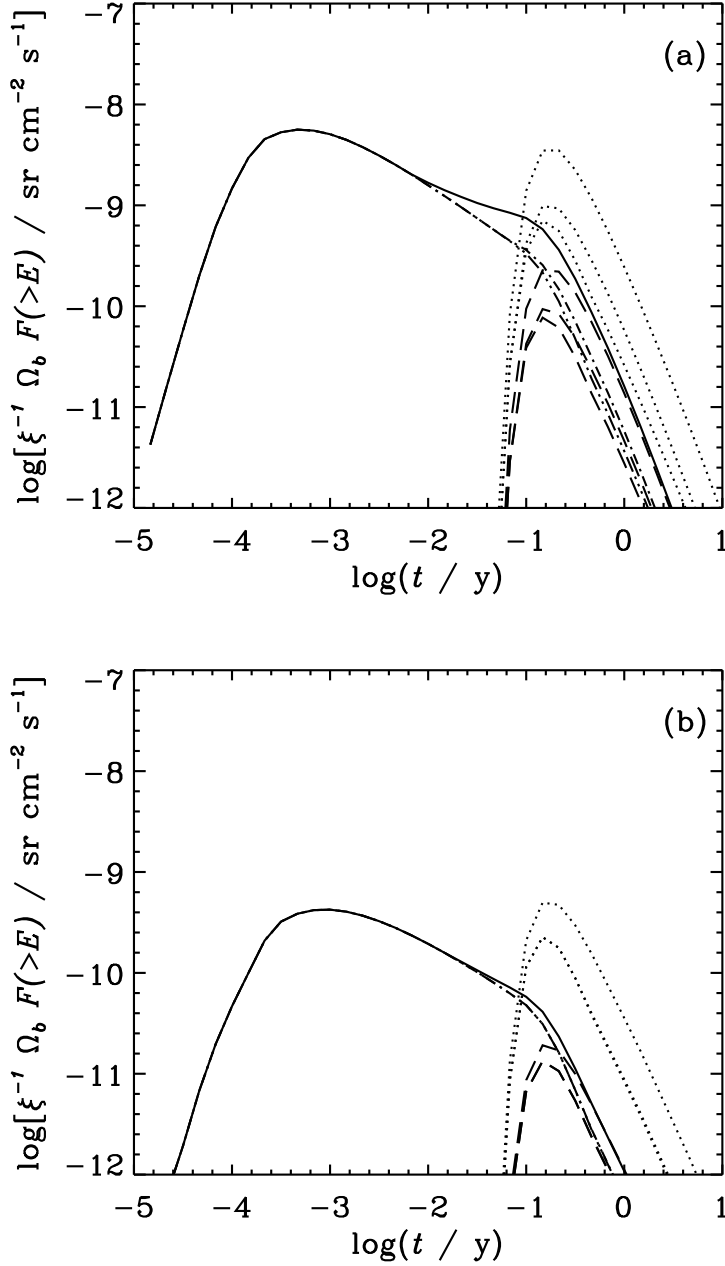


Figure 8: The dependence of the integral flux of neutrinos ( $\nu_\mu + \bar{\nu}_\mu$ ) above 1 TeV (solid, dot-dash, and dot-dot-dot-dash curves),  $\gamma$ -rays above 100 MeV (dotted curves), and  $\gamma$ -rays above 1 TeV (dashed curves) as a function of time  $t$  measured from the explosion for  $d = 10$  kpc and  $B \sin i = 10^{12}$  G and for (a)  $P_0 = 5$  ms, and (b)  $P_0 = 10$  ms. Results are shown for the three radiation field models: no polar cap heating – dot-dot-dot-dash curve and lowest dotted and dashed curves; moderate heating – dot-dash curve and middle dotted and dashed curves; maximum heating – solid curve and upper dotted and dashed curves.

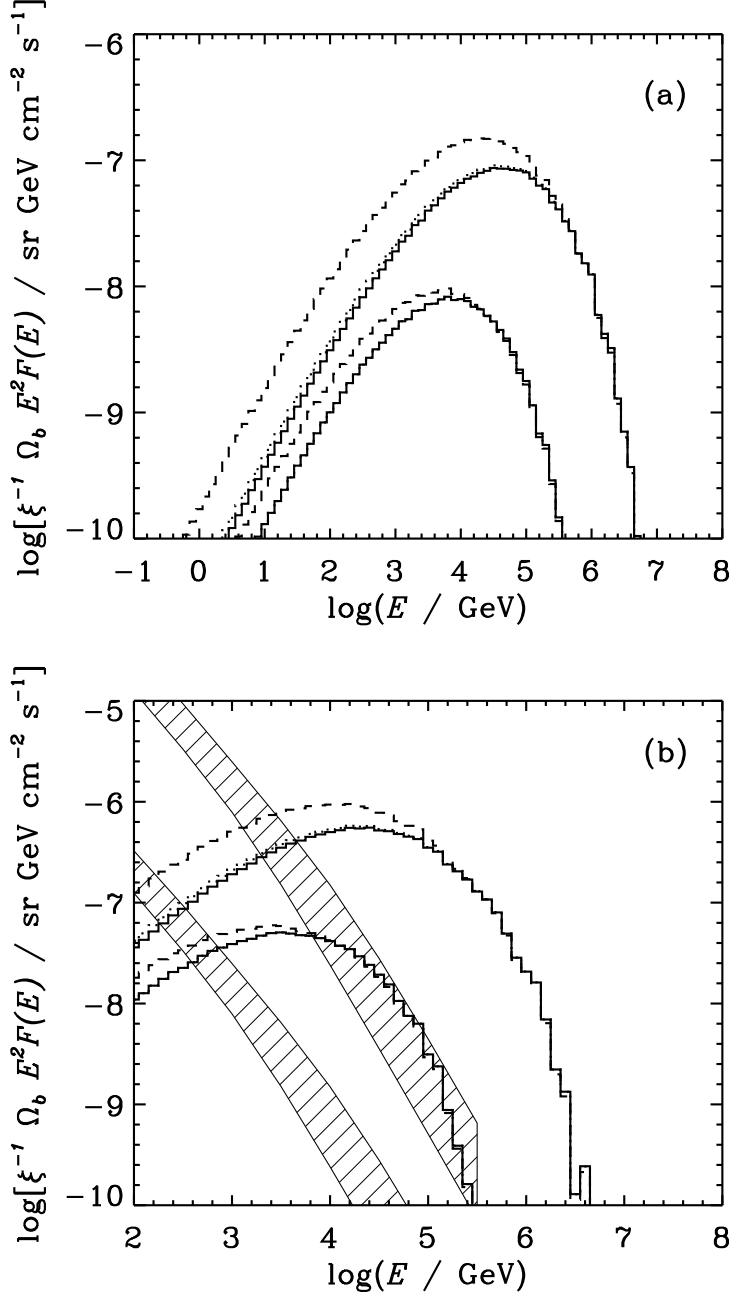


Figure 9: The spectra for  $d = 10$  kpc at  $t = 0.1$  year of (a)  $\gamma$ -rays and (b) neutrinos ( $\nu_\mu + \bar{\nu}_\mu$ ) produced by collisions of neutrons with the matter of the supernova shell. In each case, the upper three histograms are for  $P_0 = 5$  ms, and the lower three histograms for  $P_0 = 10$  ms. Results are shown for  $B \sin i = 10^{12}$  G for the three radiation field models: no polar cap heating – lower histogram; moderate heating – middle histogram; maximum heating – upper histogram. The atmospheric neutrino background flux multiplied by  $E^2$  ( $\text{GeV cm}^{-2} \text{s}^{-1}$ ) within  $1^\circ$  and within  $10^\circ$  of the source direction, based on the intensity calculated by Lipari [48], is shown by the hatched bands (each band shows the range of atmospheric neutrino background as the zenith angle changes).

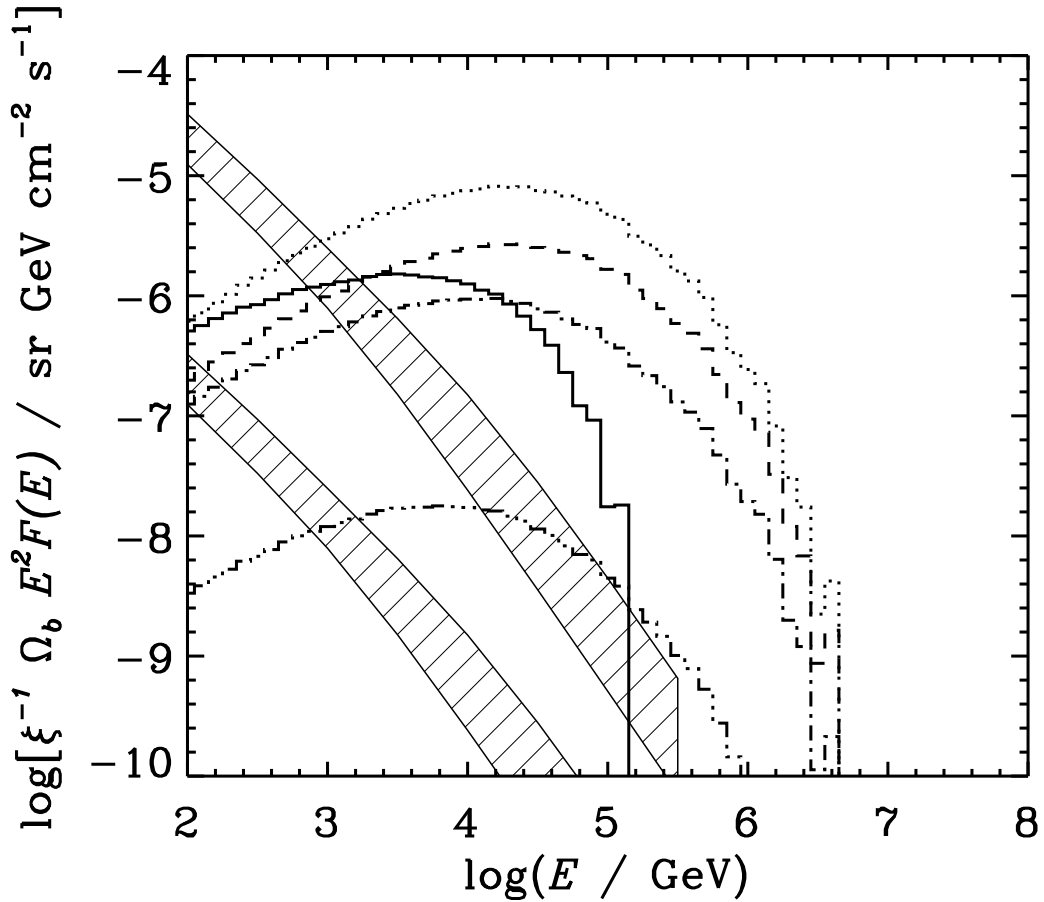


Figure 10: Evolution of the spectrum of neutrinos ( $\nu_\mu + \bar{\nu}_\mu$ ) produced by collisions of neutrons with matter in the supernova shell for  $B \sin i = 10^{12}$  G,  $P_0 = 5$  ms and the maximum polar cap heating model. Spectra are shown for  $d = 10$  kpc and for  $t = 10^{-4}$  y (solid histogram);  $10^{-3}$  y (dotted histogram);  $10^{-2}$  y (dashed histogram);  $10^{-1}$  y (dot-dash histogram); 1 y (dot-dot-dot-dash histogram). See Fig. 9 for explanation of hatched bands.